Proceedings of the ASME 2014 Dynamic Systems and Control Conference
DSCC2014
October 22-24, 2014, San Antonio, TX, USA

DSCC2014-6289

SYRINGE POSITION CONTROL FOR BACK PRESSURE MODULATED DROP VOLUME IN FUNCTIONAL INKJET PRINTING

Nikhil Bajaj
School of Mechanical Engineering
Purdue University
West Lafayette, Indiana 47907
Email: bajajn@purdue.edu

J. William Boley
School of Mechanical Engineering
Purdue University
West Lafayette, Indiana 47907
Email: jwboley@purdue.edu

Aaron Fulton
School of Mechanical Engineering
Purdue University
West Lafayette, Indiana 47907
Email: fulton@purdue.edu

George T.-C. Chiu
School of Mechanical Engineering
Purdue University
West Lafayette, Indiana 47907
Email: gchiu@purdue.edu

ABSTRACT

Inkjet printing technologies have been common and well developed over the past few decades, and more recently have gained significant acceptance in functional printing and additive manufacturing applications. Control of dot gain in the deposition process is a desirable capability for a printing system from the perspective of process control and throughput, and preliminary data suggests dot gain and drop volume can be controlled in inkjet systems through manipulation of the reservoir back pressure. In order to help facilitate further exploration, the design of a back pressure control system is proposed, and the system modeled, with linear and nonlinear control designs proposed and compared in simulation for this nonlinear plant application, where the nonlinear control design, a sliding mode controller, outperforms the tested linear control design.

NOMENCLATURE

A Syringe surface area, m^2
V_p Piping volume, m^3
V_s Syringe volume, m^3
V_t Total reservoir volume, m^3
P_R Reservoir (absolute) pressure, Pa
P_A Ambient pressure, Pa
P_b Back pressure, Pa
x Syringe deflection from initial position, m
x_0 Initial syringe position, m
$V_{t,initial}$ Total reservoir volume at $x = 0$, m^3
$P_{R,initial}$ Initial reservoir pressure, Pa
n Number of moles of gas (air), mol
R Ideal gas constant, J/(K*mol)
T Air temperature, K
K_g Gas right-hand side constant, N*m
F_s Syringe nonlinear spring force, N
F_f Syringe friction force, N
F_c Coulomb friction force, N
F_e "External force" for friction model, N
F_v Voice coil actuator force, N
F_k Voice coil spring return force, N
c Syringe viscous damping coefficient, N/(m/s)
K_c Voice coil return spring constant, N/m
m_s Syringe plunger mass, kg
m_a Voice coil armature mass, kg
m_t Total mass, kg

U Amplifier voltage, V
L Voice coil inductance, H
r Voice coil resistance, Ω
V_{bemf} Back-emf voltage, V
K_f Voice coil force constant, N/A
K_b Voice coil back-emf constant, V/(m/s)
c_a Viscous damping coefficient for actuator, N/(m/s)

INTRODUCTION

Inkjet systems are a very common class of drop-on-demand (DOD) printing system that are used for ink delivery in everyday consumer printers and are produced by a number of manufacturers, such as the Seiko Epson Corporation, Canon Inc. and the Hewlett-Packard Company. There are multiple types of inkjet technology, and the most commonly used are piezoelectric inkjet and thermal inkjet technologies.

In thermal inkjet (TIJ) systems, the print head is comprised of an array of nozzles, generally produced through lithographic micro-fabrication processes [1]. The systems integrate reservoirs of ink or other fluid behind the nozzles and eject drops on demand by pulsing resistive heating elements that are adjacent to the reservoirs with a short, intense voltage waveform. The Ohmic heating of the resistive element quickly vaporizes a small amount of the fluid and creates sufficient pressure for a drop of ink to be ejected from the nozzle. In piezoelectric inkjet systems, drops are ejected by utilizing a piezoelectric transducer arranged with a nozzle that is actuated in order to produce a tuned pressure wave through the fluid, ejecting a drop.

An important parameter in both types of process is the back pressure, or reservoir pressure, of the nozzle system. This range depends on the nozzle, and manufacturers choose a value in the range depending on fluid jettability [2] characteristics. The pressure is below ambient pressure so that even low-viscosity, low-surface tension fluids will stay in the correct area of the reservoir, while if the pressure is too far below ambient pressure it may effect nozzle refill rates and therefore the firing rate of the nozzle. However, it is well understood that for most fluid choices there is a range of back pressure values that will allow jetting of droplets.

The back pressure may also have some additional ability to effect dot gain, the size of the dots on the substrate formed through inkjet deposition, through the complex mechanisms of the inkjet process. Preliminary results for a 12-nozzle TIJ head and one particular functional ink are shown in Figure 1. This particular ink is a palladium hexadecanethiolate-based ink that exemplifies the many applications of functional printing, as it has applications in electronics fabrication and sensing application through surface-enhanced Raman spectroscopy (SERS) [3, 4]. This material and others have some challenges involved with depositing device-quality films and structures due to fluid properties [5]. While printing techniques have been developed to improve performance, additional flexibility in dot gain without having to change nozzles would be of value in such applications. Other applications, such as bioprinting [6] and sensor functionalization via inkjet [7, 8], also stand to benefit from dot gain control, as dosing control could be improved significantly.

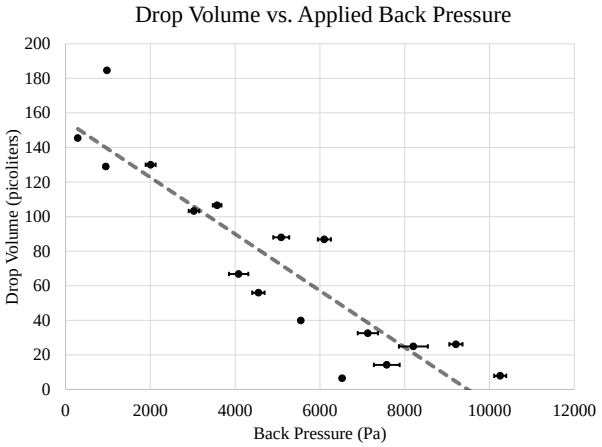

Figure 1. Drop volume vs. back-pressure for a 16-nozzle TIJ head.

For this TIJ system the back pressure for the shared reservoir for all 12 nozzles is held constant at some value that is generally in the range of 800 Pa to 10 kPa below the ambient atmospheric pressure, and a trend correlating the back pressure and drop volume is evident. The methodology of this experiment is explained in [9].

Significant work has been done modulating dot gain by waveform design in piezoelectric inkjet devices [10]. This work has been continued and well studied in multiple types of piezoelectric inkjet heads [11], and has even been implemented in commercial devices [12].

However, dot gain has not been controlled online in printing systems via back pressure, to best of the authors' knowledge, in TIJ or piezoelectric systems. This would allow additional flexibility to print control designers. In order to study this behavior and implement back pressure-modulated control of dot gain, it is desired to build a low cost back pressure control system that can vary back pressure in synchronization with an experimental inkjet printing system. The contribution of this paper is design of a robust model-based control strategy for controlling the back pressure in a syringe-based pressure control system.

SYSTEM DESCRIPTION AND MODEL DEVELOPMENT

The system that will be built to be controlled is shown in a diagrammatic form in Figure 2. The Linear Force Actuator is specified as a Motran Industries axial force transducer (model AFX70NS) rated at 70 Newtons of DC force, and 15 N/A force constant. Other important specifications from a modeling perspective are taken from the data sheet and presented in Table 1.

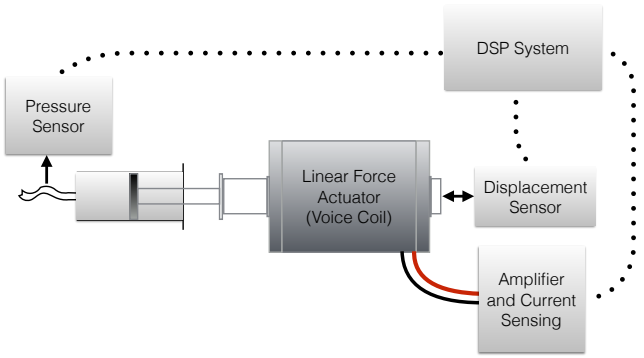

Figure 2. Schematic representation of control system.

A 3 mL Luer-lock syringe is used as the syringe portion.

The system in a schematic form can be modeled as in Figure 2. There are two main components to the dynamical behavior - the syringe dynamics and the actuator dynamics. The behavior will be derived separately, coupled through a force term, F_v that will appear on both free-body diagrams.

Syringe Behavior The free-body diagram (FBD) for the syringe is shown in Figure 3(a). The important forces are F_s, a nonlinear spring force due to the compression or expansion of the air in the reservoir, F_f, the force due to friction (from the syringe plunger in contact with the syringe walls, and F_v, the voice coil actuator force.

We assume the plunger has some small mass, m_p. Because the relative magnitude of the back pressure is very small compared to the ambient pressure, the piping is unlikely to deform significantly. For this reason, in the model the piping volume V_p is constant, and the total volume of the reservoir will be $V_p + V_s$, where V_s is the volume of the air in the syringe. This is a state dependent volume (on the position, x, offset by the initial syringe position x_0) and thus the total air volume can be written as:

$$V_t = V_p + V_s = V_p + A(x + x_0) \tag{1}$$

where A is the syringe plunger surface area. We know the ideal gas law to be:

$$PV = nRT = K_g = V_{t,initial} P_{R,initial} \tag{2}$$

In this case, n,R, and T are assumed constant, and therefore K_g is a constant. Therefore we have a relationship so that the quantity

$$P_R(x) V_t(x) = K_g = V_{t,initial} P_{R,initial} \tag{3}$$

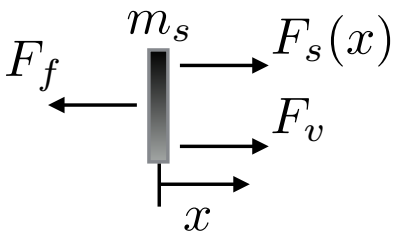

(a) Free body diagram of the syringe plunger.

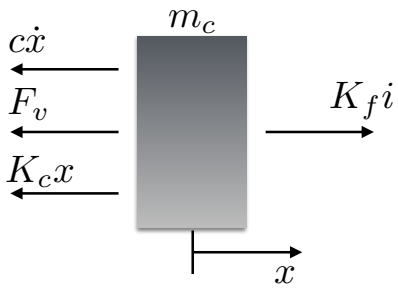

(b) Free-body diagram of actuator.

Figure 3. System free body diagrams.

with $V_{t,initial} = V_p + Ax_0$. Substituting, we can find that:

$$P_R(x) = \frac{K_g}{V_t(x)} = \frac{(V_p + Ax_0) P_{R,initial}}{V_p + A(x + x_0)} = \frac{(V_p + Ax_0) P_A}{V_p + A(x + x_0)} \tag{4}$$

because $P_{R,initial} = P_A$ by design. The back pressure, $P_b(x) = P_A - P_R(x)$ and so

$$P_b(x) = P_A - \frac{(V_p + Ax_0) P_A}{V_p + A(x + x_0)} = \frac{P_A(V_p + A(x + x_0) - P_A(V_p + Ax_0)}{V_p + A(x + x_0)} \tag{5}$$

$$= -\frac{P_A A x}{V_p + A(x + x_0)} \tag{6}$$

Equation 6 is the back pressure as a function of the position x. The backpressure will be the system output y in the state-space representation of the system. Using the back pressure P_b, we can write the nonlinear spring-like force due to the compression or expansion of the air in the reservoir by just multiplying by the area of the syringe:

$$F_s(x) = P_b(x) A = -\frac{P_A A^2 x}{V_p + A(x + x_0)} \tag{7}$$

The back-pressure $P_b(x)$ (Equation 6) and spring-like force $F_s(x)$ (Equation 7) as a function of the state x are illustrated in Figure

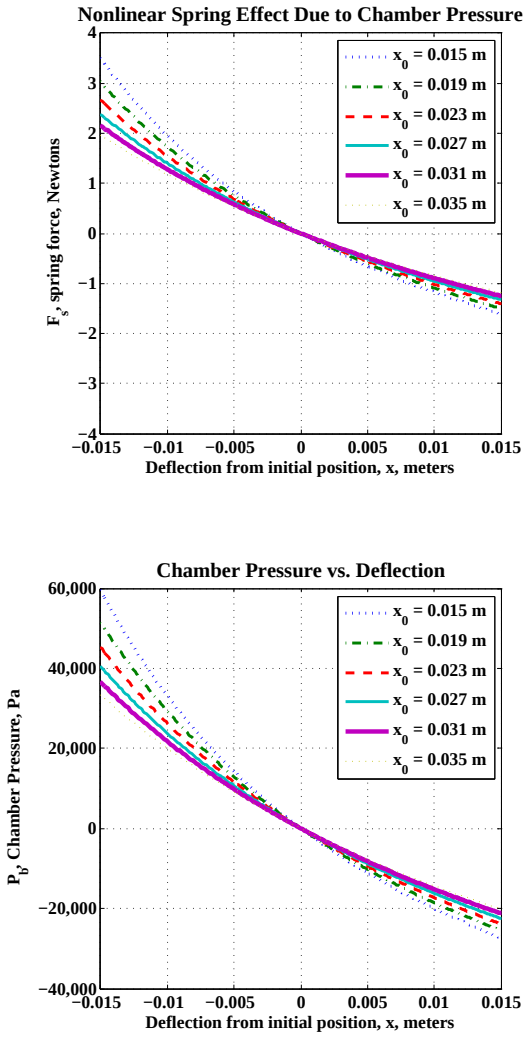

Figure 4. Nonlinear spring-like effect due to back pressure and back pressure vs. deflection with varying initial positions x_0 and assuming a typical 3 mL syringe and V_p of 1.5E-6 m^3.

4. It is clear from the figure that the back pressure is a nonlinear function of the position, and that the spring-like force is also a nonlinear effect. The friction force F_f is modeled as a Coulomb friction force with viscous damping - that is:

$$F_f(\dot{x},F_e) = \begin{cases} F_e & \dot{x}=0, |F_e| < F_c \\ F_c \operatorname{sgn}(F_e) + c\dot{x} & |\dot{x}| > 0 \end{cases} \tag{8}$$

Here, F_e is an external force equal to the sum of all other forces on the syringe, which can be written as:

$$F_e = F_v + F_s(x) \tag{9}$$

Finally, we can find that the sum of all forces for the syringe allow the dynamic relationship:

$$m_s\ddot{x} = F_v + F_s(x) - F_f \tag{10}$$

Actuator Behavior

The voice coil dynamics are very similar to those of a DC electric motor except for two differences - one, the motion occurs in a linear manner rather than rotational, and secondly, the actuator utilized here has a significant center-return spring force. We assume that the actuator shaft and the syringe shaft are rigidly connected and so the displacement of the actuator can also be taken to be x, and that this is the deviation from the center position of the voice coil. A free body diagram of the actuator rigid body is shown in Figure 3(b).

The input to the system is given as the amplifier output voltage, U. After application of Kirchoff's voltage law, it is found that the actuator is governed here by two equations:

$$m_c\ddot{x} + c_a\dot{x} = K_f i - F_v - K_c x \tag{11}$$

$$L\dot{i} + Ri = U - K_b\dot{x} \tag{12}$$

L is the coil inductance, R is the coil resistance, and K_b is the back-emf constant.

Overall System Model

Combining the syringe behavior from Eqns. 10 and 8 with the actuator behavior from Eqns. 12 and 11, the system behavior can be written as:

$$(m_s+m_c)\ddot{x} = K_f i - c_a\dot{x} - K_c x + F_s(x) - F_f \tag{13}$$

$$L\dot{i} = U - K_b\dot{x} - Ri \tag{14}$$

We will select the states x_1, x_2, x_3 to be $x, \dot{x}$, and i, respectively, with input U and output $y = P_b(x)$, as defined before, and so the system can be written in a (non-linear) state-space representation:

$$\begin{bmatrix} \dot{x_1} \\ \dot{x_2} \\ \dot{x_3} \end{bmatrix} = \begin{bmatrix} 0 & 1 & 0 \\ -\frac{K_c}{m_s+m_c} & -\frac{c_a}{m_s+m_c} & \frac{K_f}{m_s+m_c} \\ 0 & -\frac{K_b}{L} & -\frac{R}{L} \end{bmatrix} \begin{bmatrix} x_1 \\ x_2 \\ x_3 \end{bmatrix} + \begin{bmatrix} 0 \\ \frac{F_s(x_1)-F_f(x_2,F_e)}{m_s+m_c} \\ \frac{U}{L} \end{bmatrix} \tag{15}$$

Where,

$$F_f(x_2,F_e) = \begin{cases} F_e & x_2=0, |F_e| < F_c \\ F_c \operatorname{sgn}(F_e) + cx_2 & |x_2| > 0 \end{cases}$$

$$F_e = F_v + F_s(x_1)$$

$$F_v = \frac{m_s}{m_s+m_c}(K_f x_3 - c_a x_2 - K_c x_1) - \frac{m_c}{m_s+m_c}(F_s)$$

The system therefore contains a static output nonlinearity. For the purposes of this implementation, because the output nonlinearity is invertible over the operating range in the system model, the nonlinearity is used as a lookup relationship. For a given desired pressure, the required position state x_1 can be computed, and control applied on the position state.

Equilibria

The equilibria of the open loop (no input, homogenous) system can be found by setting $\dot{x_1}, \dot{x_2}, \dot{x_3} = 0$. If this is done then certainly equilibrium can only exist when $x_2, x_3 = 0$. The conditions on x_1 are due to the spring-like forces and also static friction, and they produce a range of x_1 that satisfies the equilibrium conditions. The range of x_1 is:

$$\frac{M - \sqrt{-4AK_c(-F_cV_p - AF_cx_0 + (-M)^2)}}{2AK_c} \leq x_1 \leq \frac{M + \sqrt{-4AK_c(-F_cV_p - AF_cx_0 + (-M)^2)}}{2AK_c} \quad (16)$$

where $M = AF_c - A^2P_A - K_cV_p - AK_cx_0$.

Given no input, the system will have an equilibrium in the range given in Eqn 16. In addition, intuitively the system is stable in its autonomous form, as the forces present are all attractive towards the equilibrium calculated above.

System Parameters

the following values are used for the system parameters based on design and actuator estimates.

Linear Control Design

Linear control design will be attempted by linearizing about one of the given equilibria. For simplicity we pick $x_1 = 0$, and set $F_f = 0$. Then, we can differentiate the $F_s(x_1)$ into:

$$F_s(x_1) = -A\frac{P_AAx}{V_p + A(x + x_0)} \quad (17)$$

$$\frac{d}{dx_1}F_s(x_1)|_{x_1^e=0} = \frac{A^3P_Ax_1^e}{(V_p + A(x_1^e + x_0))^2} - \frac{A^2P_A}{V_p + A(x_1^e + x_0)} = -\frac{A^2P_A}{V_p + Ax_0} \quad (18)$$

Table 1. Parameters Used in Control Design and Simulation

Parameter	Units	Value
A	m^2	5.8901E-5
V_p	m^3	1.5E-6
P_A	Pa	101000
x_0	m	0.015
F_c	N	2
c	N/(m/s)	0.01
K_c	N/m	2200
m_s	kg	0.01
m_c	kg	0.44
m_t	kg	0.45
U	V	$-10 < U < 10$ (saturation)
L	H	0.003
R	Ω	2.5
K_f	N/A	15
K_b	V/(m/s)	15
c_a	N/(m/s)	0.01

the results of this is the coefficient of the first term of the Taylor series about zero for F_s, allowing us to write that

$$F_s(x_1) \approx -\frac{A^2P_A}{V_p + Ax_0}x_1 \quad (19)$$

Full State Feedback Control

This allows us to construct the linear system in Equation 20.

$$\begin{bmatrix} \dot{x_1} \\ \dot{x_2} \\ \dot{x_3} \end{bmatrix} = \begin{bmatrix} 0 & 1 & 0 \\ -(\frac{K_c}{m_T} + \frac{A^2P_A}{V_p + Ax_0}) & -\frac{c_a}{m_T} & \frac{K_f}{m_T} \\ 0 & -\frac{K_b}{L} & -\frac{R}{L} \end{bmatrix} \begin{bmatrix} x_1 \\ x_2 \\ x_3 \end{bmatrix} + \begin{bmatrix} 0 \\ 0 \\ \frac{1}{L} \end{bmatrix} U \quad (20)$$

The output is still the nonlinear mapping from x_1 to P_b, however, this is relatively easy to compute, and for the control design the methodology will be to precompute the x_1 that corresponds to the desired setpoint in P_b. Therefore we can treat the output as $y = Cx$ with $C = [1, 0, 0]$. Given the nature of the sensing in the current application, we assume full state feedback, and with perfect measurements at this time. A gain matrix K is chosen in the conventional pole-placement technique. Eigenvalues of $(A - BK)$ were chosen to be [-100+100i, -100-100i, -350].

Integrator-Augmented Full State Feedback Control

We can also add an integrator to try to mitigate the steady-state error that would be inevitable with simply implementing full-state feedback control. The linear system is augmented to be:

$$\begin{bmatrix} \dot{x_1} \\ \dot{x_2} \\ \dot{x_3} \\ \dot{w} \end{bmatrix} = \begin{bmatrix} 0 & 1 & 0 & 0 \\ -(\frac{K_c}{m_T} + \frac{A^2 P_A}{V_p + A x_0}) & -\frac{c_a}{m_T} & \frac{K_f}{m_T} & 0 \\ 0 & -\frac{K_b}{L} & -\frac{R}{L} & 0 \\ 1 & 0 & 0 & 0 \end{bmatrix} \begin{bmatrix} x_1 \\ x_2 \\ x_3 \\ w \end{bmatrix} + \begin{bmatrix} 0 \\ 0 \\ \frac{1}{L} \\ 0 \end{bmatrix} U \tag{21}$$

A gain matrix K is chosen in the conventional pole-placement technique. Eigenvalues of $(A - BK)$ were chosen to be [-100+100i, -100-100i, -300, -400].

Linear Control Performance Results

Performance results for the chosen designs are shown in Figure . When the linearized system is simulated with the chosen control gains, the system performs well (the state feedback, linear simulation (SFL) case). However, when the state feedback controller without augmentation is applied to the nonlinear system, there is significant steady state error due to the static friction effect as well as the nonlinear spring effect. This is also why the steady state error can actually overshoot the setpoint in the cases when the system is traveling a farther distance, and why the steady state error is not always the same percentage of the setpoint as would be the case in a linear system with a constant disturbance. This can be seen in the state feedback with nonlinear plant (SFNL) case.

The integrator resolves the steady state error issue and the performance is relatively good, as seen in the augmented state feedback with linear plant (ASFL) case. However, in the augmented state feedback with nonlinear plant case (ASFNL) it is slower to converge than one would expect based on the linear design simulation, and exhibits significant overshoot that would not be predicted based on linear design methods. Tuning of the pole locations could improve performance somewhat in overall settling time, but rise time would be difficult to improve without inducing more oscillatory behavior.

Nonlinear Control Design

In order to take advantage of our understanding of the nonlinear system (and not just treat the nonlinearities as disturbances or uncertainties to a linear system) it is desirable to implement a nonlinear control scheme to potentially improve performance [13]. For certain classes of voice coil actuator, methods such as sliding mode control (SMC) have been utilized in the past to deal with nonlinear friction effects and improve tracking speed and precision. In this system, the nonlinear spring effect also can be addressed through a robust control method such as SMC,

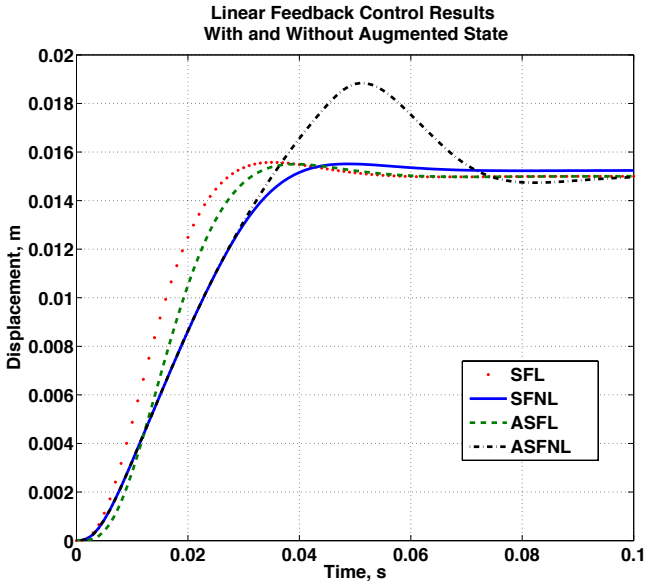

Figure 5. Linear design performance results. SFL: state feedback, linear simulation. SFNL: state feedback, nonlinear simulation. ASFL: augmented state feedback, linear simulation. ASFNL: augmented state feedback, nonlinear simulation.

without adding an integrator that could slow down response or impact stability.

Sliding Mode Control

To make mathematical simplification more straightforward, we will, without loss of generality and in complete equivalence, absorb the viscous damping term from F_f into c_a making a new viscous damping term $\hat{c} = c_a + c$. F_f changes to $\hat{F_f}$:

$$\hat{F_f}(\dot{x}, F_e) = \begin{cases} F_e & \dot{x} = 0, |F_e| < F_c \\ F_c \operatorname{sgn}(F_e) & |\dot{x}| > 0 \end{cases} \tag{22}$$

For simplification of notation, let us make the following notation changes:

$$\begin{aligned} \lambda &= -\hat{c}/m_t \\ \alpha &= -K_c/m_t \\ \beta &= K_f/m_t \\ \gamma(x_1) &= F_s(x_1)/m_t \\ q &= -\hat{F_f}/m_t \\ p &= -K_b/L \\ \mu &= -R/L \end{aligned}$$

The new state space equations, including these substitutions, become:

$$\dot{x_1} = x_2 \tag{23}$$
$$\dot{x_2} = \lambda x_2 + \alpha x_1 + \beta x_3 + \gamma(x_1) + q \tag{24}$$
$$\dot{x_3} = p x_2 + \mu x_3 + U/L \tag{25}$$

Following the method of [14] and [15] we would like to choose a sliding function:

$$s = x_2 - g x_3 - h x_1 \tag{26}$$

We will select g and h later. We now would like to choose U such that it drives the states to the sliding surface, $s = 0$. According to Lyapunov stability theory, this can be accomplished if U is selected such that $s\dot{s} = -\varepsilon|s|$ for $\varepsilon > 0$ and $s \neq 0$. Taking the derivative of the sliding function and substituting,

$$\dot{s} = \dot{x_2} - g\dot{x_3} - h\dot{x_1} \tag{27}$$
$$= (\lambda - gp - h)x_2 + (\beta - g\mu)x_3 + \alpha x_1 + \gamma(x_1) + q - gU/L \tag{28}$$

If we choose

$$U = \frac{L}{g}((\lambda - gp - h)x_2 + (\beta - g\mu)x_3 + \alpha x_1 + n^+ s) + \frac{L}{g} l^+ \operatorname{sgn}(s) \tag{29}$$

where n^+ and l^+ are positive constants, then,

$$\dot{s} = -l^+ \operatorname{sgn}(s) - n^+ s + \gamma + q \tag{30}$$

This implies that:

$$s\dot{s} = -l^+ s \operatorname{sgn}(s) - n^+ s^2 + \gamma s + qs \tag{31}$$
$$\leq -l^+|s| + |\gamma s| + |qs| \tag{32}$$
$$\leq -(l^+ - |\gamma| - |q|)|s| \tag{33}$$

Noting that we know the bounds for γ of which the largest in absolute value is γ_{max}, and that we know that the maximum value of q is given by $F_c/m_t = q_{max}$, choosing

$$l^+ = \varepsilon + \frac{F_c}{m_t} + \gamma_{max} \tag{34}$$

Will satisfy the requirement that was

$$s\dot{s} \leq -(l^+ - |\frac{-1}{m_t}||F_c - (\gamma(x_1)|)|s| < -\varepsilon|s| \tag{35}$$

We now have 3 remaining control variables to assign: n^+, g, and h. On the sliding surface, $s = 0$, and so,

$$x_2 - g x_3 - h x_1 = 0 \rightarrow x_3 = \frac{x_2}{g} - \frac{h x_1}{g} \tag{36}$$

Therefore the state space system can be rewritten as second-order:

$$\begin{aligned} \dot{x_1} &= x_2 \\ \dot{x_2} &= \lambda x_2 + \alpha x_1 + \frac{\beta}{g} x_2 - \frac{h}{g}\beta x_1 + \gamma + q \end{aligned} \tag{37}$$

This can then be rewritten as:

$$\ddot{x_1} = (\lambda + \frac{\beta}{g})\dot{x_1} + (\alpha - \frac{h\beta}{g})x_1 + \gamma + q \tag{38}$$

Taking the Laplace transform and rearranging,

$$\begin{aligned} &S^2 X_1(S) - \left(\frac{\beta}{g} + \lambda\right) X_1(S) - \left(\alpha - \frac{h\beta}{g}\right) X_1(S) \\ &= S x_1(0) + \dot{x_1}(0) - \left(\lambda + \frac{\beta}{g}\right) x_1(0) + \mathcal{L}[\gamma + q] \end{aligned} \tag{39}$$

where S is the Laplace variable. Solving for $X_1(S)$ yields:

$$\begin{aligned} X_1(S) = &\frac{S x_1(0) + \dot{x_1}(0) - \left(\frac{\beta}{g} + \lambda\right) x_1(0)}{S^2 - \left(\frac{\beta}{g} + \lambda\right) S + \left(\frac{h\beta}{g} - \alpha\right)} \\ &+ \frac{\mathcal{L}[\gamma + q])}{S^2 - \left(\frac{\beta}{g} + \lambda\right) S + \left(\frac{h\beta}{g} - \alpha\right)} \end{aligned} \tag{40}$$

Assume that the characteristic equation of Equation 40 has double roots of $-k < 0$. Then the steady stated time domain solution to Equation 40 can be bounded by:

$$\begin{aligned} &|x_1(\infty)| \leq \\ &b_1 e^{-kt} + b_2 t e^{-kt} + \left| \int_0^\infty (q_{max} + \gamma_{max})(t - \tau)\tau e^{-k\tau} d\tau \right| \\ &\leq \int_0^\infty |(q_{max} + \gamma_{max})(t - \tau)| \left| \tau e^{-k\tau} \right| d\tau \\ &\leq |(q_{max} + \gamma_{max})| \int_0^\infty \tau e^{-k\tau} d\tau \\ &= |(q_{max} + \gamma_{max})| \left(\frac{\tau e^{-k\tau}}{k} - \frac{e^{-k\tau}}{k^2} \right) \Big|_0^\infty \\ &= \frac{|(q_{max} + \gamma_{max})|}{k^2} \end{aligned} \tag{41}$$

This steady state value is what we would like to eliminate and therefore based on requirements and known values of q_{max} and γ_{max} we can select k. Once k is known, g and h can be chosen due to the double root choice. Any n^+ should result in eventually reaching the sliding surface, though intuitively looking at Equation 27 the larger that n^+ is, the faster the system should reach the sliding surface. For simplicity we will also choose $n^+ = k$. From the characteristic equation:

$$S^2 - \left(\frac{\beta}{g} + \lambda\right) S + \left(\frac{h\beta}{g} - \alpha\right) = S^2 + 2kS + k^2 = 0 \qquad (42)$$

From this, clearly $g = -\beta/(2k+\lambda)$ and $h = -(k^2+\alpha)/(2k+\lambda)$.

Sliding Mode Control Results

The sliding mode controller was implemented using the same input parameters as the linear controllers. $|\gamma_{max}|$ is taken to be (3.5 N / 0.445 kg) = 7.865 N/kg. F_c = 2 N, and so $|q_{max}|$ = 2 N / 0.445 kg) = 4.944 N/kg. Therefore, for a steady-state error of 0.00005 meters, or 50 microns, $k = \sqrt{(4.994 + 7.865)/.00005} =$ 507.15. 50 microns was here chosen as a design parameter based partially on the expected encoder resolution, as the expect resolution is 12.5 microns.

These parameters were used in a MATLAB [16] implementation of the sliding mode controller, using the equation derived here. The dynamics were simulated using a 4th-order Runge-Kutta solver.

Given these quantities, h, g, and therefore U can be computed, allowing the controller to be implemented. Results are shown for a 15 mm step in Figure . The sliding mode control system has better performance than the linear system. A slew rate-like saturation behavior can be seen, which is present for both the sliding mode controller and the augmented linear one. This is likely due to both tuning and the fact that the sliding mode controller could operate at saturation in an intelligent and robust manner, whereas linear controllers can struggle when saturating. Saturation at the beginning of a transient may speed up the response time but ultimately lead to dangerous oscillations or overshoot, which is in this case less of a problem with the sliding mode control system. The difference in the steady-state control voltage value is due to static friction. This was determined by setting the static friction force F_c to zero and performing the same step motions. In that case, the final steady state value for both the linear controller with the integrator and for the sliding mode controller were the same.

Conclusions

The sliding mode controller seems like a promising method for controlling this nonlinear system with higher performance

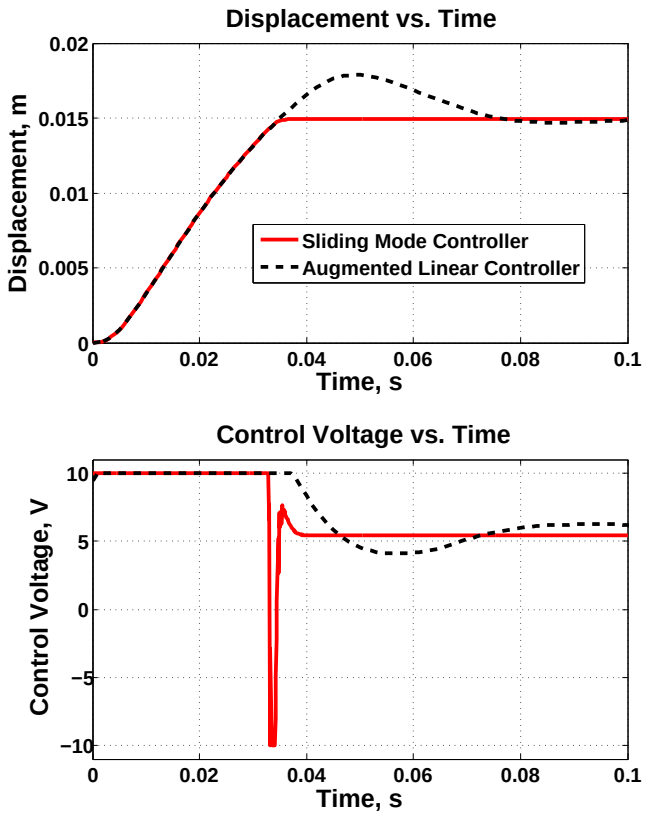

Figure 6. Sliding mode control performance for a 15 mm step vs. linear state feedback controllers.

than is achievable with linear control designs. It is possible that when the system is implemented on a real system that additional disturbances like noise, along with implementation in discrete rather than continous time, could cause chattering issues with the sliding mode controller. Advancements that could be made on this work would be implementing a smoothed sliding mode control to help mitigate such issues. A further improvement to the system would be to incorporate the output nonlinearity into the control design. The control system, once tuned, then needs to be integrated into a printing system, and the overall printing system control architecture will require careful design to best take advantage of the high performance possible with this back pressure controller.

REFERENCES

[1] Hess, U., 1988. Integrated thermal ink jet printhead and method of manufacture, Jan. 12. US Patent 4,719,477.

[2] Derby, B., 2010. "Inkjet printing of functional and structural materials: Fluid property requirements, feature stability, and resolution". *Annual Review of Materials Research,* **40**(1), pp. 395–414.

[3] Bhuvana, T., Boley, W., Radha, B., Dolash, B., Chiu, G., Bergstrom, D., Reifenberger, R., Fisher, T., and Kulkarni, G., 2010. "Inkjet printing of palladium alkanethiolates for facile fabrication of metal interconnects and surface-enhanced raman scattering substrates". *Micro Nano Letters, IET,* **5**(5), October, pp. 296–299.

[4] Bhuvana, T., and Kulkarni, G. U., 2008. "A sers-active nanocrystalline pd substrate and its nanopatterning leading to biochip fabrication". *Small,* **4**(5), pp. 670–676.

[5] Boley, J. W., Shou, C., McCarthy, P., Fisher, T., and T.C.-Chiu, G. "The role of coalescence in inkjet printing functional films: An experimental study". *NIP & Digital Fabrication Conference,* **2013**(2), pp. 508–513.

[6] Derby, B., 2012. "Printing and prototyping of tissues and scaffolds". *Science,* **338**(6109), pp. 921–926.

[7] Post, N. J., 2007. "Precision micro-deposition of functional layers using inkjet drop-on-demand and applications to the functionalization of microcantilever sensors". Master's thesis, Purdue University, West Lafayette.

[8] Kumar, V., Boley, J. W., Yang, Y., Ekowaluyo, H., Miller, J. K., Chiu, G. T.-C., and Rhoads, J. F., 2011. "Bifurcation-based mass sensing using piezoelectrically-actuated microcantilevers". *Applied Physics Letters,* **98**(15).

[9] Boley, J. W., 2013. "Print mask design for inkjet functional printing". PhD thesis, Purdue University, West Lafayette.

[10] Chen, A. U., and Basaran, O. A., 2002. "A new method for significantly reducing drop radius without reducing nozzle radius in drop-on-demand drop production". *Physics of Fluids (1994-present),* **14**(1), pp. L1–L4.

[11] Castrejón-Pita, A. A., Castrejón-Pita, J. R., and Martin, G. D., 2012. "A novel method to produce small droplets from large nozzles". *Review of Scientific Instruments,* **83**(11).

[12] Rensch, C., 2006. Creation of small microdrops. Tech. rep., MicroFab Technologies, Inc.

[13] Khalil, H. K., 2001. *Nonlinear Systems (3rd Edition)*, 3 ed. Prentice Hall, Dec.

[14] Tsai, C.-L., Lee, T.-C., and Lin, S.-K., 2009. "Friction compensation of a mini voice coil motor by sliding mode control". In Industrial Electronics, 2009. ISIE 2009. IEEE International Symposium on, pp. 609–614.

[15] Slotine, J.-J. E., and Li, W., 1991. "Applied nonlinear control". *NJ: Prentice-Hall, Englewood Cliffs*.

[16] MATLAB, 2013. *version 8.1.0 (R2013a)*. The MathWorks Inc., Natick, Massachusetts.